Hindawi
Geofluids
Volume 2022, Article ID 7502693, 12 pages
https://doi.org/10.1155/2022/7502693

Research Article

Finite Element Study on Temperature Field of Underwater Dredging Devices via the Artificial Ground Freezing Method

Yuwei Wu,[1,2] **Hui Zeng**,[1] **Jun Hu**,[1,2] **Xingyue Ren**,[2] **and Xiang Xue**[3]

[1]*School of Civil Engineering and Architecture, Wuyi University, Jiangmen, Guangdong 529020, China*
[2]*School of Civil Engineering and Architecture, Hainan University, Haikou 570228, China*
[3]*Hainan Environmental Geological Exploration Institute, Sanya 57200, China*

Correspondence should be addressed to Hui Zeng; zeng202110@126.com and Jun Hu; hj7140477@hainanu.edu.cn

Received 24 February 2022; Revised 15 April 2022; Accepted 30 April 2022; Published 7 June 2022

Academic Editor: Dongdong Ma

Increased urbanization has led to undesirable increases in the discharge of refuse waste and pollutants in urban and rural rivers. Blockages and river pollution adversely affect navigation and aquatic ecosystems and cause flooding during the flood season. Regular riverbed dredging is essential to protect local ecosystems and maintain waterways' health. However, the current dredging methods cause secondary pollution during dredging. This study examined a new river dredging method with a parametric analysis of its reliability for different construction environments. ADINA software solved the temperature field model using the finite element method to build a three-dimensional transient heat conduction model. The analysis determined the distribution and development of the temperature field during the freezing process and the effective dredging range of the frozen device. We compared thermal conductivities, specific heat capacities, freezing device sizes, initial ground temperatures, and brine cooling plans to examine the effect of the soil's thermophysical properties and construction environment on the dredging area of the freezing device.

1. Introduction

The unreasonable development pace of construction projects accelerates the urbanization process, affecting river operation and development, requiring the clearing of the rivers of debris, garbage, and silt, which negatively impact the river ecosystem, endangering the safety and health of urban residents. The accumulation of more muck in the river channel raises the riverbed level, thus affecting the river channel's flood control and drainage functions. As the river channel reaches the downstream, silt progressively precipitates and jeopardizes the river channel flow, causing flood disasters during the flood season due to blockage.

Furthermore, high sediment concentrations are flushed downstream and partially deposited in inundated areas [1] or other slow-flowing regions, such as inland harbors and harbor entrances. Therefore, inland ports become partly inaccessible for navigation, which are essential for economic growth. For example, harbor entrances are completely impassible, and goods cannot be shipped. However, waterways must be navigable all year. Therefore, regular maintenance such as dredging is needed [2].

Typically, dredging involves three stages (extraction, transportation, and disposal), and each step requires the use of different technologies. Various dredgers used in the extraction and transportation stages include cut-suction dredgers and trailer-mounted dredgers [3]. Contaminated dredged materials are generally discarded at sea or recycled for beneficial use. Contaminated materials, on the other hand, require specialized treatment. Dredging has a significant environmental impact, including increased turbidity, organic compounds, and metal compounds in the dredged sediments and water [4–6]. According to [7], dredging is a commercial activity that causes considerable environmental damage. The stirring of sediments releases pollutants, and the aquatic environment's physical, chemical, and biological properties will change accordingly [8–10]. However, the dredging process helped ships navigate and allowed them to enter ports more efficiently and develop. As a result, the

environmental harm caused needs urgent study. Many studies have investigated the environmental impact of dredging activities [11–16] and their implications [17, 18]. However, only a few studies consider how to mitigate the environmental impacts of dredging (e.g., [12]). Hu outlined an idea concerning a device design based on artificial ground freezing (AGF) for salvaging or sampling underwater sediments that were both economical and environmentally sustainable [19]. By combining the impenetrable characteristics of ice with the strength of the frozen ground, AGF was often used to create a hydraulic barrier that strengthens and stabilizes the ground structure while controlling groundwater movement, a typical civil engineering practice in shaft sinking, underground uranium mining, hazardous waste containment, and other environmental projects [20]. In AGF, the ground temperature dropped to a level below the freezing point of groundwater. A possible way to circulate a coolant with a subzero temperature over the targeted area was extracting heat from deep within the ground layers and eventually turning the groundwater into ice. It showed that most dredging processes previously studied had significant secondary environmental impacts. Thus, this paper is aimed at developing a numerical model to qualitatively explore the dredging effect of a new environmentally friendly dredging equipment based on Hu's new concept. And on this basis, various thermodynamic parameters are examined for their impact on the dredging effect to use the article results as a reference for applying this new technology to engineering problems.

This paper introduces the AGF application into the dredging process with a parametric analysis of a series of influencing factors, including thermal parameters, the construction conditions, and the geometry size of the freezing device. In addition, by analyzing the evolution of the temperature field change pattern, this paper attempts to determine the frozen device's frozen range and its dredging efficiency. Finally, the study provides some insights into the introduction of AGF as a construction technique for river dredging.

2. Model Developed

Figure 1 shows an artificial freezing plate comprising a steel plate shell, a frozen pipe, and thermal insulation materials. The frozen pipe was close to the device's bottom. Thermal insulation material restrained heat transfer between the frozen pipe and the top side of the freezing apparatus. As a result, the recirculation of outflowing brine occurred in the thermostatic bath machine, where it cooled, maintaining the freezer plate at a low temperature enabling the frozen material and the freezer plate to be brought out of the water together.

Figure 2 gives the flowchart of the entire AGF construction process. The freezing dredging process began by marking the target location of the operation, outlining the installation environment for measurements, followed by the installation of freezing equipment, the freezing and temperature regulation systems, and the active freezing process of installing the frozen pipe. Next, we removed the lifting

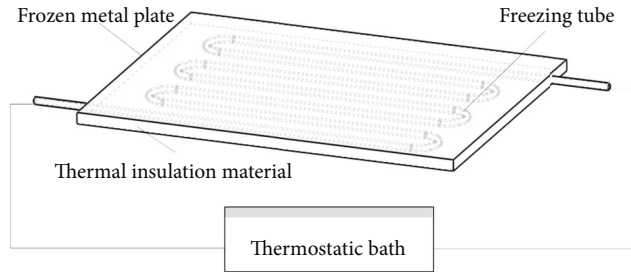

Figure 1: Schematic of the freezing device.

points on the dredging and salvage device's freezing plat at the end of the freezing process to complete the dredging and salvage operation. Then, the removed underwater dredging and fishing device was reusable.

3. Materials and Methods

Numerical modeling techniques simulated the dynamic temperature evolution around the freezing dredge device to evaluate the efficiency of the proposed device.

3.1. Numerical Simulation. Compared with heat conduction in the heat transfer process, convection and radiation in the freezing process are less. Hence, we applied the Fourier equation to describe the freezing process following the principle of energy conservation. As a result, the parabolic partial differential equation written below was followed [21]:

$$\frac{\partial}{\partial \mathrm{x}}\left(k\frac{\partial T}{\partial x}\right)+\frac{\partial}{\partial y}\left(k\frac{\partial T}{\partial y}\right)+\frac{\partial}{\partial z}\left(k\frac{\partial T}{\partial z}\right)+q^{v}=c\frac{\partial T}{\partial t}, \quad (1)$$

where K is the thermal conductivity, T is the temperature, c is the specific heat capacity of the solid per unit volume, and t is the time.

3.1.1. Assumptions. We formulated the process as a two-dimensional transient with simultaneous heat flows in the freezing process. In developing the analysis, we made the following assumptions:

(i) The soil layer was uniformly heated, taking 18°C as its initial temperature. As a result, the constant temperatures in the soil layer ranged from 15°C to 20°C within 10 meters underground (i.e., within 10 meters underground at 15°C to 20°C); the soil was a homogeneous, continuous, and isotropic entity

(ii) The temperature load was applied directly to the bottom of the artificial freezing plate or the wall of the frozen pipe

(iii) Considering that the upper part of the artificial freezing device had insulating materials, convection caused by temperature and heat radiation caused by soil resistance were minimal and therefore neglected in the simulation; additionally, thermal resistance on heat conduction was also small and overlooked

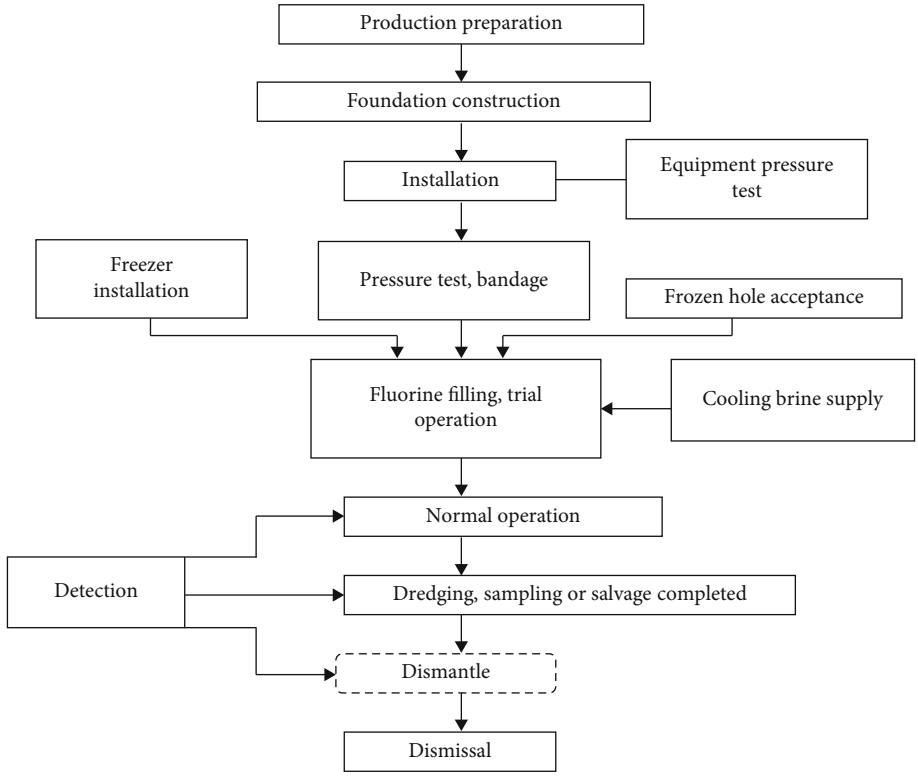

Figure 2: Flowchart for the AGF process.

(iv) The freezing temperature of the soil layer was -1°C; i.e., the range of the -1°C isotherm envelope was the maximum freezing area obtained after considering some undesirable factors, i.e., the full dredging range. On the other hand, the temperature at which the soil layer formed a stable frozen soil curtain was -10°C, that is, the scope of the -10°C isotherm envelope being the minimum freezing area obtained after considering various unfavorable factors, such as the minimum dredging range

(v) We assumed that the soil layer's density, specific heat capacity, and thermal conductivity were constants. Next, separately consider the soil layer's frozen and nonfrozen states. Each state was independent of the other

3.1.2. Geometric Model, Meshes, and Layout of Observation Paths. Figure 3(a) depicts the grid division of the artificial freezing device and the soil model. The numerical simulation considered phase change based on a transient three-dimensional heat conduction model. The commercial ADINA software assisted in solving the numerical model. The dimensions of the model were 30 m (length) × 14 m (width) × 15 m (height). The freezing device and the soil model had a 4-node meshing method. The mesh density setting for the soil boundary part was 1 m, while the mesh density of the artificial freezing device was 0.5 m.

Figure 3(b) illustrates the observation path and the observation point in this study. Set up observation paths: path 1 (vertical downward observation path starting from the center of the freezing plate, one observation point for each 0.5 m, six observation points in total) and paths 2 to 4 (horizontal observation paths, located 0.5 m, 1.5 m, and 2 m below the center of the freezing plate, respectively, one observation point every 0.5 m, six observation points on each path).

3.1.3. Soil Properties and Boundary Conditions. Sandy clay widely occurred in the riverbeds and was used as an example for testing the freezing device's efficiency. The thermodynamic parameters of the soils used in this study are presented in Table 1.

The formation's initial temperature before freezing was 18°C. Next, the thermal load (brine temperature) was set at the surface of the dredging device. Finally, the planned brine temperature was loaded directly onto the dredging device as the temperature load [22]. An adiabatic boundary surrounded the soil used to bury the dredging device. Figure 4 gives the temperature curves used in this case. All the other sides were adiabatic. The temperature-time curve was discretized to individual load steps. Each step had several substeps, and we applied an iterative algorithm in each substep. In this study, the time step was one day (24 hours), and the total period for active freezing and maintenance freezing was 40 days.

4. Effective Dredge Area Susceptibility to Different Conditions

Considering the complexity of this underwater freezing problem, different construction environments and construction

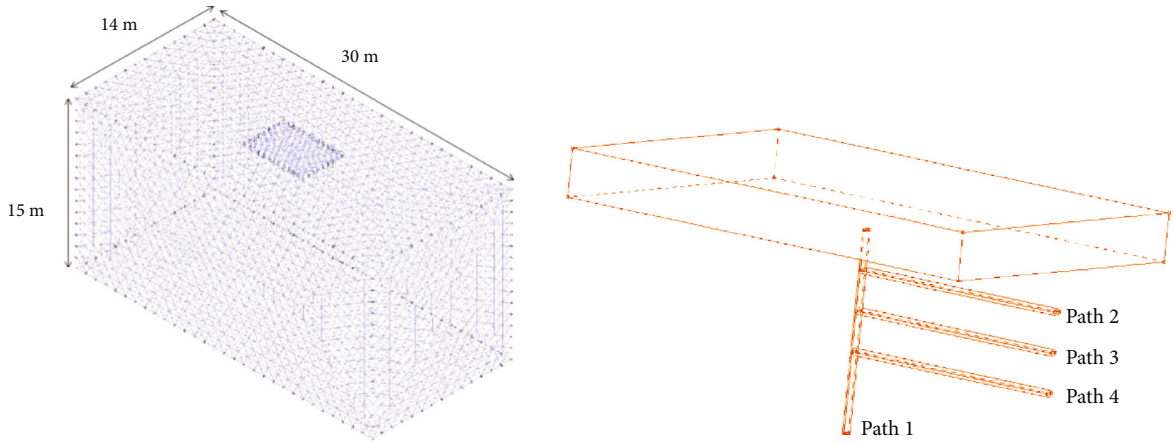

(a) Mesh computational domain and boundary (b) Observation path

Figure 3: Schematic of the freezing device.

Table 1: Soil parameters.

Porosity ($kg \times m^{-3}$)	Thermal conductivity ($kJ \times m^{-1} \times °C^{-1}$)		Heat capacity ($kJ \times m^{-1} \times °C^{-1}$)		Latent heat ($\times 10^8$ J/m^3)
	Unfrozen soil	Frozen soil	Unfrozen soil	Frozen soil	
1.880	118	179	1.53	1.61	1.20

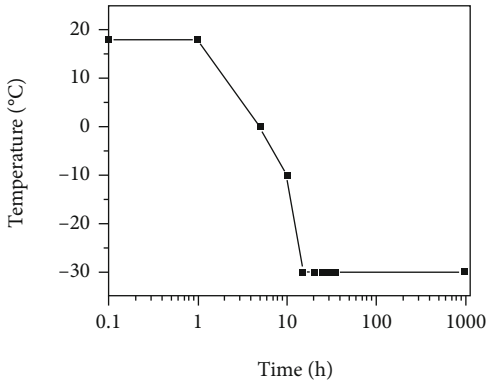

Figure 4: The applied boundary temperature curve.

conditions can significantly affect the freezing process. Consequently, we studied the thermal range and dredging of the frozen slab range under various factors, examining throughout this section how the geometry size of the freezing devices, thermal conductivities, specific heat capacities, soil types, initial ground temperatures, and brine cooling plans affect the effective dredging range.

4.1. Effect of Geometry Size. The size of the freezing device directly impacted the frozen contact area during the freezing process. Consequently, examining the development of the temperature field of the soil during the freezing process for different geometries of freezing devices was critical, providing a better understanding of the influence of this factor on the dredges' range. There were four different sizes of freezing devices used in this study, as shown in Table 2.

Table 2: The geometry of the freezing device.

Number	Height (m)	Width (m)	Length (m)
a	0.6	6.0	6
b	0.6	6.0	4
c	0.6	8.0	4
d	0.6	12.0	4

Figure 5 shows a cross section of the temperature distribution cloud plot at the end of freezing for freezing devices of different geometrical sizes. Again, we noted that the temperature distribution patterns were similar for the different sizes of the freezing plates and that the larger sizes did not freeze deeper for the same cooling plan.

At the end of freezing, isotherms were at -1°C and -10°C for each of the four different geometries of freezing devices to directly observe and compare the temperature distribution and effective frozen range, as shown in Figure 6.

Figure 6 shows that the change in the side length of the freezing plate had little impact on the final frozen depth. The -1°C isotherm developed to approximately 1 meter underwater after 40 days of active freezing, and the -10°C isotherm developed to about 0.6 meters underwater. The dredging device had a single row of freezing tubes. Notably, a previous study [23–25] gave a comparably similar answer for the freezing depth range for single tubes. Therefore, it verified the reliability of the calculation of this temperature field. Thus, the geometric size of the artificial freezing plate appeared to have no significant relationship with the freezing depth. The different lengths

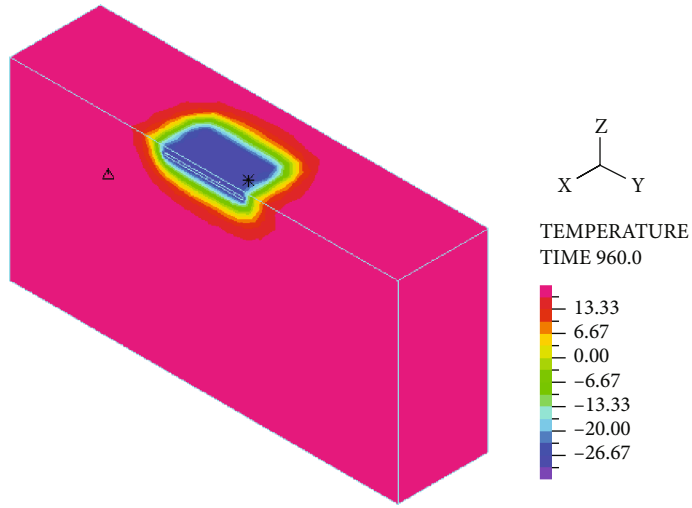

(a)

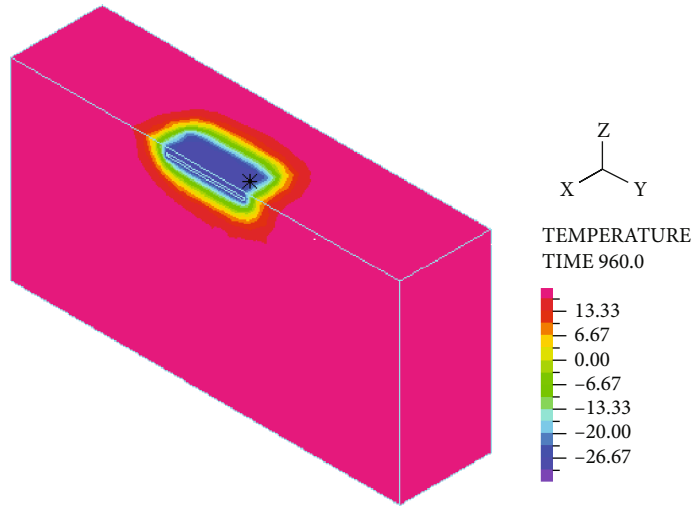

(b)

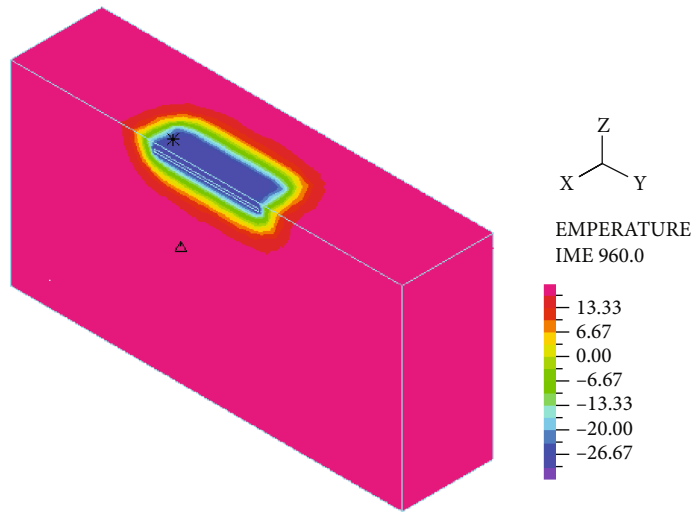

(c)

Figure 5: Continued.

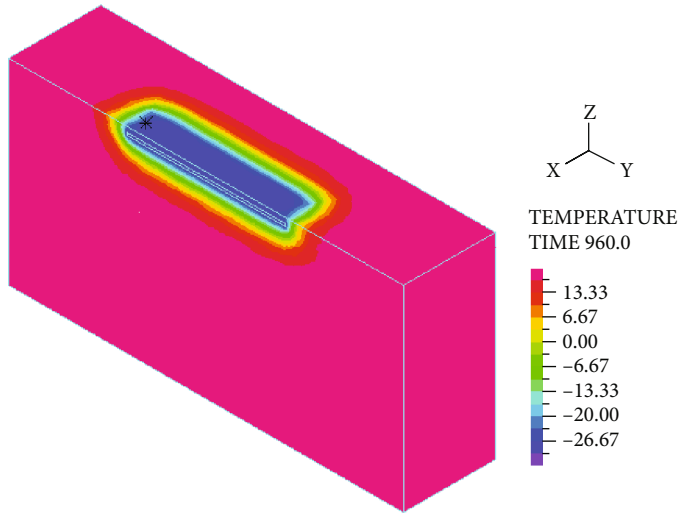

(d)

Figure 5: Schematic diagrams of the freezing devices.

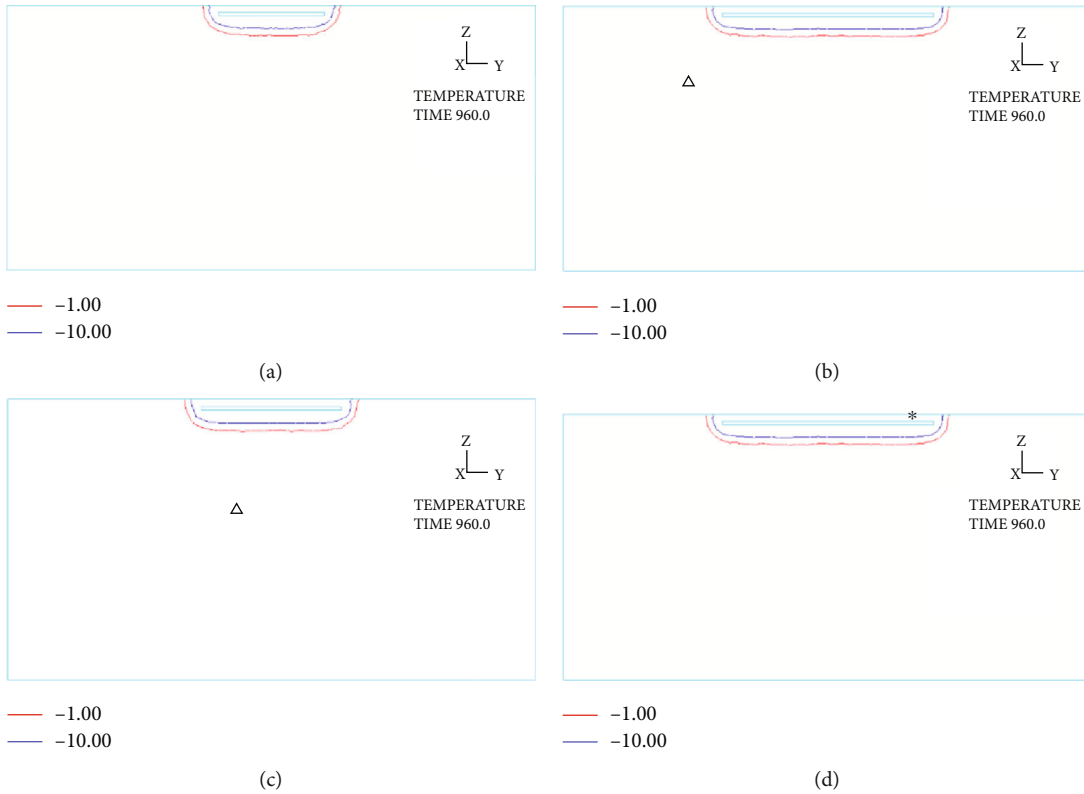

Figure 6: Schematic of the freezing device.

used with the same brine cooling plan, the development, and the change of the temperature field of the frozen plate were very similar. As a result of the limited freezing range of the freezing tube, changing the geometric size of the freezing devices may only change the frozen area but not the depth of the frozen area. However, the geometric size of the freezing device cannot change the depth of dredging, only its location.

4.2. Effect of Latent Heat. Observation point 2 on path 1, located one meter below the freezing device, was selected to monitor temperature development with time. Observe the temperature development at observation point 2 for the latent heat effects by increasing and decreasing by 10%, 20%, and 30%, respectively. The temperature development curves for other latent heat versus temperatures are in Figure 7, and it shows that different latent heats do not

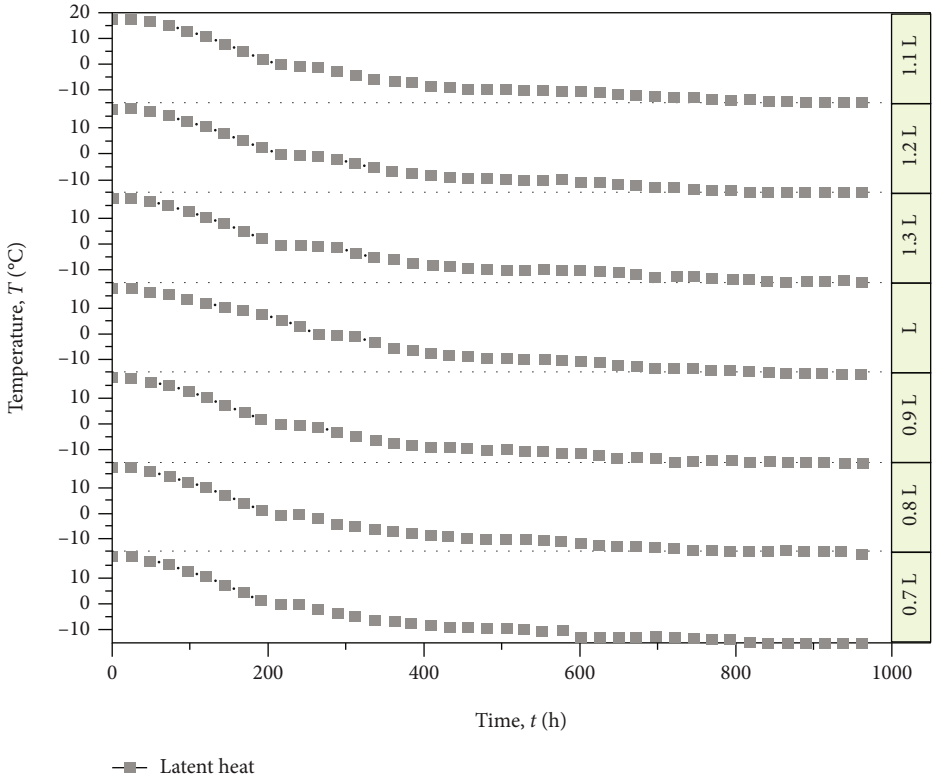

Figure 7: Schematic of the freezing device.

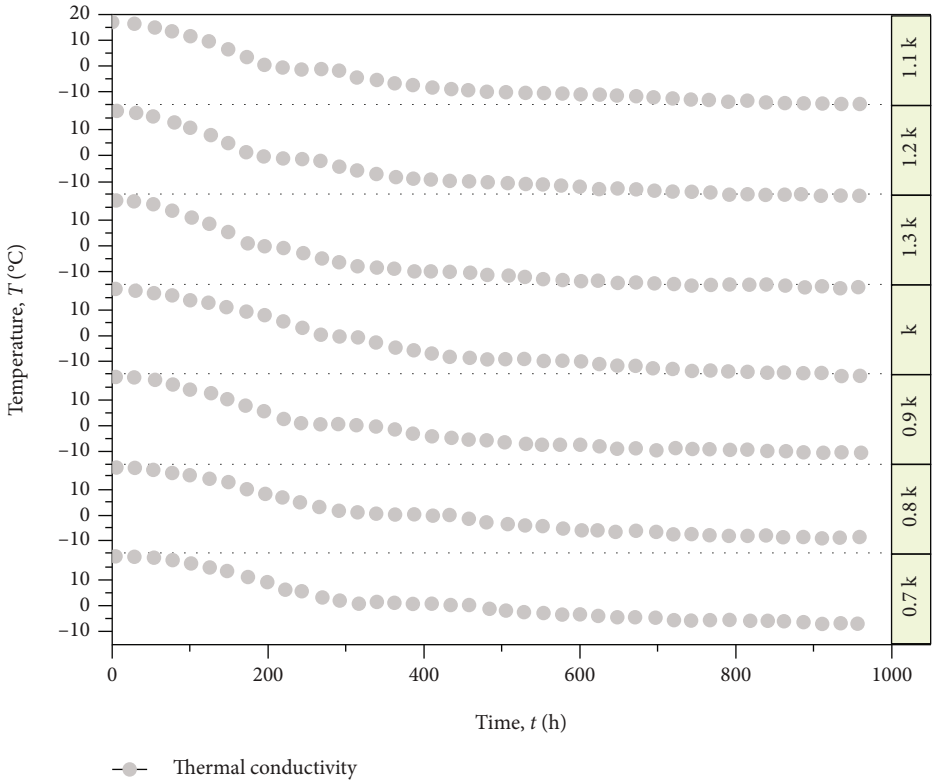

Figure 8: Effect of thermal conductivity on temperature field development.

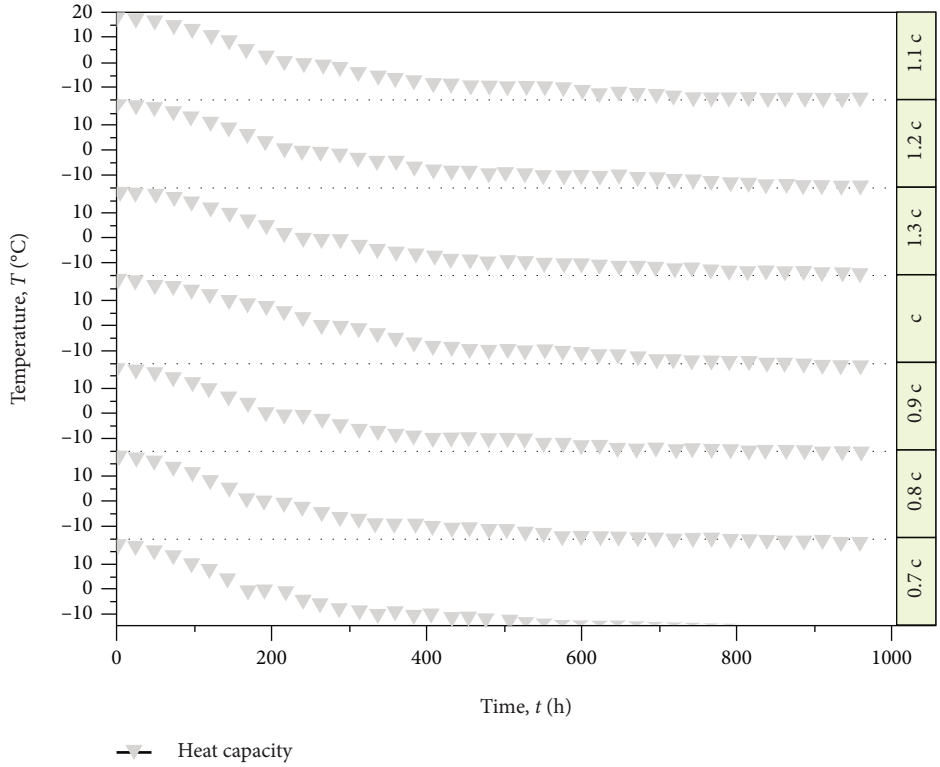

Figure 9: Effect of heat capacity on temperature field development.

Table 3: Parameters of soil material.

Soil type	Porosity ($kg \times m^{-3}$)	Thermal conductivity ($kJ \times m^{-1} \times °C^{-1}$)		Heat capacity ($kJ \times m^{-1} \times °C^{-1}$)		Latent heat ($\times 10^8$ J/m^3)
		Unfrozen soil	Frozen soil	Unfrozen soil	Frozen soil	
Cement-admixed sandy clay	2.04	200	225	1.58	1.6	0.81
Sandy clay (original)	1.880	118	179	1.53	1.61	1.20
Cement admixed soft clay	1.80	158	170	1.66	1.52	1.0
Soft clay	1.69	105	126	1.71	1.69	1.22

significantly affect temperature development. After freezing, the temperatures at observation point 2 reach close to the same value for the different latent heats.

In contrast, the temperature curve stagnates longer when freezing reaches 0 degree for soils with higher latent heat since larger latent heats consume more thermal energy to achieve the ice-water phase change. However, the difference in latent heat had little effect on the dredging efficiency of freeze dredging. Those findings are relatively consistent with those of [26, 27], which investigated the effects of different thermal parameters, including thermal conductivity and latent heat, on the freezing of a shield-driven tunnel and a cup-shaped wall. However, we observed that the freezing effect in these studies depended on the soil's thermal conductivity but not on its latent heat.

4.3. Effect of Thermal Conductivity. We further explore the effects of thermal conductivity on temperature development. Thermophysical parameters such as thermal conductivity played an essential role in analyzing soil heat conduction and heat retention [28]. Since engineering projects require a detailed understanding of thermal conductivity values and thermal responses under different environmental conditions, it would be very beneficial to study the thermal conductivity of soils and how they affect temperature variations [29]. In this study, the thermal conductivity was increased and reduced by 10%, 20%, and 30%, respectively.

As shown in Figure 8, there is a clear correlation between thermal conductivity and temperature. A more excellent thermal conductivity will enable the soil to reach the freezing temperature required by the project in a shorter time, therefore improving the efficiency of the dredging process. We noted that when the thermal conductivity is reduced by 30 during the freezing process, it takes about 240 hours for observation point 2 to reach 0°C. It takes ten days for the water to freeze to 1 meter below the freezing device. It takes

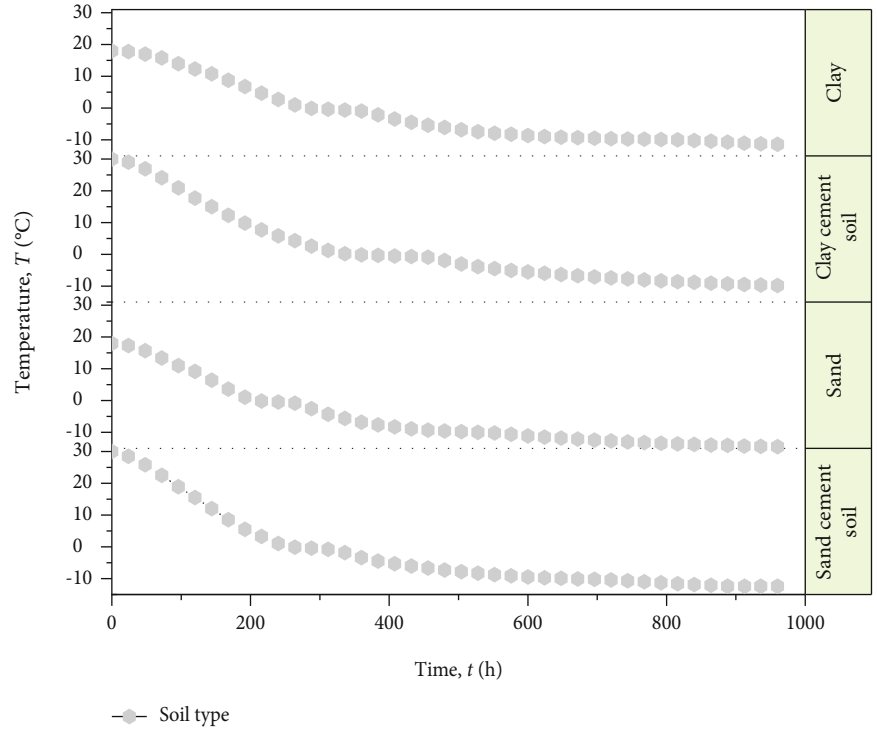

Figure 10: Effect of soil type on temperature field development.

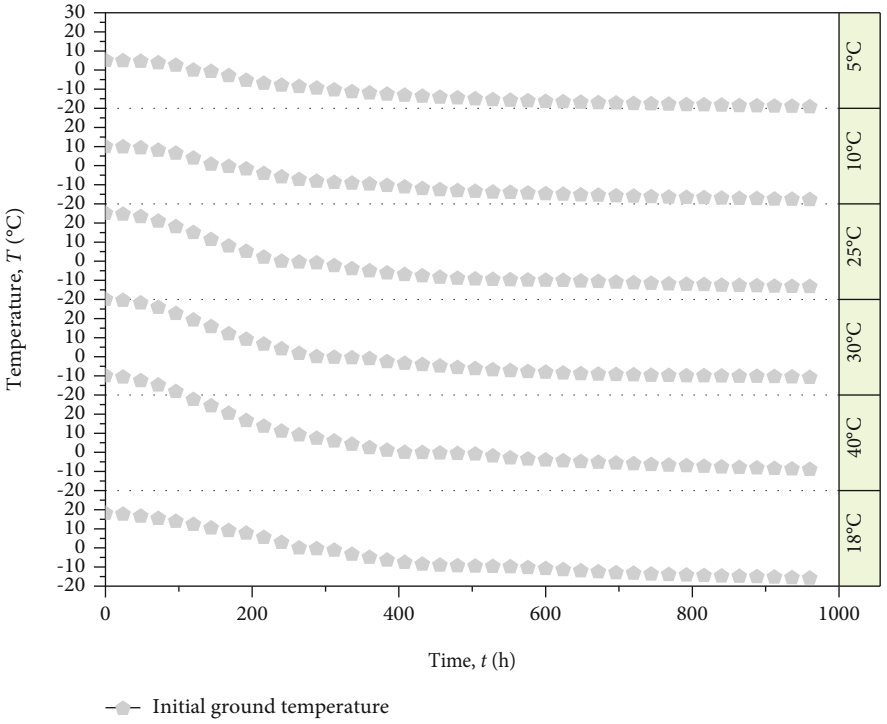

Figure 11: Effect of initial ground temperature on temperature field development.

approximately 180 hours to achieve the same frozen depth when the thermal conductivity increases by 30%. By increasing the thermal conductivity, the freezing time at the same observation point can be shortened by 60 hours, improving the freezing efficiency significantly. Therefore, during the design process, the underwater soil layer should be appropriately treated to increase its thermal conductivity and thus enhance the efficiency of the dredging project.

Table 4: Different brine cooling schedules.

Time (day)	0	1	5	10	15	20	30	960
Plan 1 (°C)	18	0	-10	-10	-10	-10	-10	-10
Plan 2 (°C)	18	0	-10	-20	-20	-20	-20	-20
Plan 3 (°C)	18	0	-10	-30	-30	-30	-30	-30
Plan 4 (°C)	18	0	-10	-40	-40	-40	-40	-40

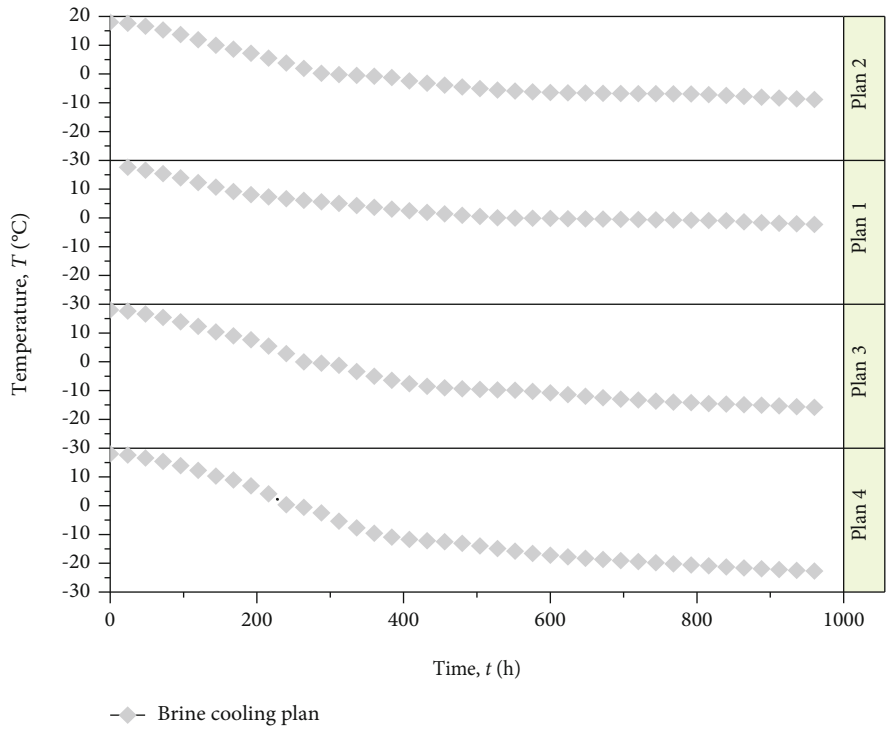

Figure 12: Effect of brine cooling plan on temperature field development.

4.4. Effect of Heat Capacity. Another factor that played a similar role in thermal conductivity was heat capacity. Heat capacity is known to result in temperature development variation. In this study, the specific heat capacity was increased and decreased by 10%, 20%, and 30%, respectively, to examine the temperature field under different conditions.

Figure 9 shows the temperature profile at observation point 2 for different heat capacities. As the heat capacity decreases, the temperature at observation point 2 decreases. It is because soils with a lower heat capacity tend to conduct temperature more quickly, thus causing the temperature under the freezing device to freeze more quickly. For example, when the heat capacity is reduced by 30%, it takes about 150 h to reach 0°C at observation point 2 and about 340 h to drop to -10°C. When the heat capacity increases by 30%, it takes about 250 h to cool down to 0°C at observation point 2 and about 500 h to cool down to -10°C. Thus, soil with a lower heat capacity can be more easily frozen and dredged than soil with a higher specific heat capacity.

4.5. Effect of Soil Type. Table 3 gives the thermal and other properties of the four soils studied. These soils were sandy clay, cement-admixed sandy clay, soft clay, and cement admixed soft clay. The laboratory-measured thermal properties were from studies [22, 24, 26, 30] that also discussed different soils to determine thermal field development.

As shown in Figure 10, different soil types exhibit other temperature change profiles at observation point 2. As a result of the cement's heat of hydration, the initial freezing temperature of the cement-treated soil is relatively high, and therefore, it takes longer for the ground to fall to 0 or -10 degrees compared to the uncemented earth. As can be seen from the comparison between clay and sand soils, the sand freezes more rapidly as compared to clay, where a cooling time to 0°C is 300 hours and a cooling time to -10°C is 600 hours and requires only 200 hours to reach 0°C and 450 hours to achieve -10°C. Thus, cement-treated soils were not conducive to more efficient dredging, whereas freeze dredging was more efficient in the sand than in clay.

4.6. Effect of Initial Ground Temperature. The construction environment will significantly affect the temperature field and the soil's natural characteristics. Figure 11 illustrates the effect of the initial temperature on the development of

the temperature field. At observation point 2, the temperature changes are discussed at initial ground temperatures of 5, 10, 18, 25, 30, and 40 degrees.

As shown in Figure 11, the temperature trends at observation point 2 were similar for different initial ground temperatures. The higher the initial temperature, the longer it took to cool down to 0 degrees at 1 m below the freezing device. The effective freezing range of the frozen slab was reached at a depth of 1 m below the frozen slab at 970 h for all different initial temperatures.

4.7. Effect of Brine Cooling Plan. The brine cooling schedule will also affect temperature development. Therefore, four different brine cooling schedules (presented in Table 4) were such that the initial ground temperature and freezing time were the same and the final freezing temperatures of -10, -20, -30, and -40 degrees were used to study the effects of the different brine cooling schedules on the development of the temperature field. Figure 12 illustrates the temperature development at observation point 2 under different brine cooling schedules.

Figure 12 illustrates that different brine cooling schedules significantly impact freezing efficiency. When the final freezing temperature is -10 degrees, it took 500 h to freeze to 0 degrees at observation point 2, while the lowest temperature measured in this case was -2.5 degrees, indicating no formation of an effective freezing zone 1 m below the freezing slab. At a freezing temperature of -20°C, it takes 300 h and 970 h to freeze to 0°C and -10°C, respectively, at observation point 2. At a freezing temperature of -30°C, it takes 270 h and 500 h to reduce the temperature to 0°C and -10°C, respectively, at observation point 2. At a freezing temperature of -40°C, it takes only 240 h and 350 h to reduce the temperature to 0°C and -10°C, respectively, at observation point 2. Therefore, we obtained the brine cooling schedule affecting the freezing efficiency and the dredging range. When the final freezing temperature was high, the dredging range accordingly reduced due to the limited freezing thickness of the soil. Conversely, the freezing efficiency increased when the final freezing temperature was lower in the brine cooling schedule, and the frozen depth increased, increasing the dredging range.

5. Conclusions

We developed a three-dimensional model to simulate saturated soil freezing on one side as a function of soil temperature. The influences of soil type, heat capacity, latent heat, thermal conductivity, and brine cooling plan are all considered. The conclusion can be drawn from the previous study as follows.

(1) The size of the freezing plate had almost no influence on the frozen depth. Therefore, the frozen depth was nearly the same for different geometry-shaped freezing plate sizes under the same brine cooling plan

(2) Thermal conductivity significantly influenced soil freezing, and as thermal conductivity increased, soil cooling accelerated

(3) The effect of phase changes in latent heat on soil freezing is quite limited

(4) The final freezing temperature is dependent on the brine cooling plan: before 0°C, the impact of the brine cooling plan was minimal. However, below 0°C, the final freezing temperature falls as the minimum cooling temperature decreases

(5) The artificial freezing effect in various soils also differed noticeably. For example, a cement treatment can result in a more significant freezing impact and a faster cooling process for sandy soils and soft clays

Data Availability

The data that support the findings of this study are openly available.

Conflicts of Interest

The authors declare that they have no conflicts of interest.

Acknowledgments

This research was funded by the characteristic innovation (Natural Science) projects of scientific research platforms and scientific research projects of Guangdong Universities in 2021(Grant No. 2021KTSCX139), the Natural Science Foundation of Hainan Province (No. 519MS024), the High Technology Direction Project of the Key Research & Development Science and Technology of Hainan Province, P. R. China (Grant No. ZDYF2021GXJS020), and the Natural Science Foundation of Hainan Province Youth Fund Project (421QN0964). The authors also acknowledge support from the China Scholarship Council Project (201907565040).

References

[1] H. Prazan, "Über Schwebstoffablagerungen in den Stauräumen der Donaukraftwerke in Österreich," *Österreichische Wasserwirtschaft*, vol. 42, pp. 73–84, 1990.

[2] S. E. Darby and C. R. Thorne, "Fluvial maintenance operations in managed alluvial rivers," *Aquatic Conservation: Marine and Freshwater Ecosystems*, vol. 5, no. 1, pp. 37–54, 1995.

[3] J. Lefever and E. V. Wellen, "Cutter suction dredger for dredging ground and method for dredging using this cutter suction dredger," WO2011117204A1, 2011.

[4] K. Ljung, F. Maley, and A. Cook, "Canal estate development in an acid sulfate soil—implications for human metal exposure," *Landscape and Urban Planning*, vol. 97, no. 2, pp. 123–131, 2010.

[5] M. Munawar, W. P. Norwood, L. H. McCarthy, and C. I. Mayfield, "In situ bioassessment of dredging and disposal activities in a contaminated ecosystem: Toronto Harbour," *Hydrobiologia*, vol. 188-189, no. 1, pp. 601–618, 1989.

[6] G. Wu, J. de Leeuw, A. K. Skidmore, H. H. T. Prins, and Y. Liu, "Concurrent monitoring of vessels and water turbidity enhances the strength of evidence in remotely sensed dredging impact assessment," *Water Research*, vol. 41, no. 15, pp. 3271–3280, 2007.

[7] J. G. S. Pennekamp, R. J. C. Epskamp, W. F. Rosenbrand, A. Mullié, G. L. Wessel, and V. Oord-ACZ, "Turbidity caused by dredging; viewed in perspective," *Terra et Aqua*, 1996.

[8] S. Hossain, B. D. Eyre, and L. J. McKee, "Impacts of dredging on dry season suspended sediment concentration in the Brisbane River estuary, Queensland, Australia," *Estuarine, Coastal and Shelf Science*, vol. 61, no. 3, pp. 539–545, 2004.

[9] S. Nayar, B. P. L. Goh, L. M. Chou, and S. Reddy, "In situ microcosms to study the impact of heavy metals resuspended by dredging on periphyton in a tropical estuary," *Aquatic Toxicology*, vol. 64, no. 3, pp. 293–306, 2003.

[10] D. J. Wildish and M. L. H. Thomas, "Effects of dredging and dumping on benthos of Saint John Harbour, Canada," *Marine Environmental Research*, vol. 15, no. 1, pp. 45–57, 1985.

[11] V. N. de Jonge, H. M. Schuttelaars, J. E. E. van Beusekom, S. A. Talke, and H. E. de Swart, "The influence of channel deepening on estuarine turbidity levels and dynamics, as exemplified by the Ems estuary," *Estuarine, Coastal and Shelf Science*, vol. 139, pp. 46–59, 2014.

[12] X. Ji, Y. Ma, G. Zeng et al., "Transport and fate of microplastics from riverine sediment dredge piles: implications for disposal," *Journal of Hazardous Materials*, vol. 404, no. Part A, p. 124132, 2021.

[13] H. Liu, K. Xu, and C. Wilson, "Sediment infilling and geomorphological change of a mud-capped Raccoon Island dredge pit near Ship Shoal of Louisiana shelf," *Estuarine, Coastal and Shelf Science*, vol. 245, p. 106979, 2020.

[14] E. Menegbo, "Locational analysis of surface water quality, sediment and dredge spoil at Nembe, Bayelsa State, Nigeria," *International Journal of Environment and Geoinformatics*, vol. 6, no. 1, pp. 15–21, 2019.

[15] D. S. van Maren, T. van Kessel, K. Cronin, and L. Sittoni, "The impact of channel deepening and dredging on estuarine sediment concentration," *Continental Shelf Research*, vol. 95, pp. 1–14, 2015.

[16] C. Wienberg and A. Bartholomä, "Acoustic seabed classification in a coastal environment (outer Weser Estuary, German Bight)—a new approach to monitor dredging and dredge spoil disposal," *Continental Shelf Research*, vol. 25, no. 9, pp. 1143–1156, 2005.

[17] M. Monge-Ganuzas, A. Cearreta, and G. Evans, "Morphodynamic consequences of dredging and dumping activities along the lower Oka estuary (Urdaibai Biosphere Reserve, southeastern Bay of Biscay, Spain)," *Ocean & coastal management*, vol. 77, pp. 40–49, 2013.

[18] B. Prause, E. Rehm, and M. Schulz-Baldes, "The remobilization of Pb and Cd from contaminated dredge spoil after dumping in the marine environment," *Environmental Technology Letters*, vol. 6, no. 1-11, pp. 261–266, 1985.

[19] J. Hu, "Underwater artificial freezing plate: China," 2015, Patent 201521125662.8 issued 2015-12-30.

[20] M. A. Alzoubi, M. Xu, F. P. Hassani, S. Poncet, and A. P. Sasmito, "Artificial ground freezing: a review of thermal and hydraulic aspects," *Tunnelling and Underground Space Technology*, vol. 104, p. 103534, 2020.

[21] T. N. Narasimhan, "Fourier's heat conduction equation: history, influence, and connections," *Reviews of Geophysics*, vol. 37, no. 1, pp. 151–172, 1999.

[22] Y. Liu, J. Hu, H. Xiao, and E. J. Chen, "Effects of material and drilling uncertainties on artificial ground freezing of cement-admixed soils," *Canadian Geotechnical Journal*, vol. 54, no. 12, pp. 1659–1671, 2017.

[23] Y. Fu, J. Hu, J. Liu, S. Hu, Y. Yuan, and H. Zeng, "Finite element analysis of natural thawing heat transfer of artificial frozen soil in shield-driven tunnelling," *Advances in Civil Engineering*, vol. 2020, Article ID e2769064, 18 pages, 2020.

[24] J. Hu, Y. Liu, Y. Li, and K. Yao, "Artificial ground freezing in tunnelling through aquifer soil layers: a case study in Nanjing metro line 2," *KSCE Journal of Civil Engineering*, vol. 22, no. 10, pp. 4136–4142, 2018.

[25] R. Lackner, A. Amon, and H. Lagger, "Artificial ground freezing of fully saturated soil: thermal problem," *Journal of Engineering Mechanics*, vol. 131, no. 2, pp. 211–220, 2005.

[26] J. Hu, Y. Liu, H. Wei, K. Yao, and W. Wang, "Finite-element analysis of heat transfer of horizontal ground-freezing method in shield-driven tunneling," *International Journal of Geomechanics*, vol. 17, no. 10, article 04017080, 2017.

[27] Y. Liu, K.-Q. Li, D.-Q. Li, X.-S. Tang, and S.-X. Gu, "Coupled thermal–hydraulic modeling of artificial ground freezing with uncertainties in pipe inclination and thermal conductivity," *Acta Geotechnica*, vol. 17, no. 1, pp. 257–274, 2022.

[28] K.-Q. Li, D.-Q. Li, and Y. Liu, "Meso-scale investigations on the effective thermal conductivity of multi-phase materials using the finite element method," *International Journal of Heat and Mass Transfer*, vol. 151, p. 119383, 2020.

[29] Y. Shen, Y. Wang, X. Zhao, G. Yang, H. Jia, and T. Rong, "The influence of temperature and moisture content on sandstone thermal conductivity from a case using the artificial ground freezing (AGF) method," *Cold Regions Science and Technology*, vol. 155, pp. 149–160, 2018.

[30] J. Zhao, P. Yang, and L. Li, "Investigating influence of metro jet system hydration heat on artificial ground freezing using numerical analysis," *KSCE Journal of Civil Engineering*, vol. 25, no. 2, pp. 724–734, 2021.